Metal screening effect on energy levels at metal/organic interface: Precise determination of screening energy using photoelectron and inverse-photoelectron spectroscopies

Takumi Aihara,[1] Syed A. Abd-Rahman,[1] and Hiroyuki Yoshida[2,3,*]

[1]*Graduate School of Science and Engineering, Chiba University, 1-33 Yayoi-cho, Inage-ku, Chiba 263-8522, Japan*

[2]*Graduate School of Engineering, Chiba University, 1-33 Yayoi-cho, Inage-ku, Chiba 263-8522, Japan*

[3]*Molecular Chirality Research Center, Chiba University, 1-33 Yayoi-cho, Inage-ku, Chiba 263-8522, Japan*

(Received 1 March 2021; revised 2 July 2021; accepted 6 July 2021; published 11 August 2021)

The energy level alignment at the metal/organic interface greatly affects the charge injection/extraction efficiency of electrodes in organic semiconductor devices. The charge carrier in the vicinity of the metal surface should be stabilized by the screening effect of the metal surface, thereby resulting in the narrowing of the energy gap (highest occupied molecular orbital (HOMO)–lowest unoccupied molecular orbital (LUMO) gap) and modifying the energy level alignment at the metal/organic interface. However, this metal screening effect has not been fully clarified because there has been no precise way to quantitatively evaluate the experimental values. In this study, we employed ultraviolet photoelectron spectroscopy (UPS), metastable atom electron spectroscopy (MAES), and low-energy inverse photoelectron spectroscopy (LEIPS) to examine the quasi–layer-by-layer grown film of perylene-3,4,9,10-tetracarboxylic dianhydride (PTCDA) on the atomically flat metal surface of Ag(111) and Au(111). By applying a procedure we established recently, we precisely evaluated the energy of the metal screening effect. The results demonstrate that the screening effect of the metal surface modifies the charge injection/collection barrier at the metal/organic interface by as much as 0.25 eV. We found that the PTCDA thickness dependent screening effect is precisely reproduced by the image charge model.

DOI: 10.1103/PhysRevB.104.085305

I. INTRODUCTION

Organic semiconductor devices are heralded as next-generation devices due to their unique physical properties, such as flexibility and light weight as well as applicability to low-cost solution processes in manufacturing. In these devices, the energy level alignment at the metal/organic interface is crucial to the charge injection/collection efficiency of the electrodes [1–11]. Recent organic light-emitting diodes (OLEDs) are composed of multilayered structures to maximize the charge injection efficiency [12]. A recent study also suggested that two-dimensional materials can be inserted between the metal and organic semiconductors to manipulate the charge injection/collection barrier [13].

The energy level alignment has been investigated for decades mainly using ultraviolet photoelectron spectroscopy (UPS). The formation of an interfacial dipole layer [1], energy level pinning at the Fermi level [2,3], and band bending [3] have been proposed and verified. The energy level alignment at the metal/organic interface can also be affected by the screening effect of the metal surface [4–11]. The charge in the organic layer is stabilized owing to the screening effect and, as a result, the energy gap of the organic semiconductor is narrowed near the metal surface. As the relative permittivity of organic semiconductors generally ranges between 3 and 4 [14], the screening effect of the metal surface is larger than the polarization of the organic layer. However, the previous UPS experimental studies could not quantify the screening effect because UPS only detected the occupied levels [highest occupied molecular orbital (HOMO) levels] and therefore could not distinguish the screening effect from band bending [15,16].

The screening effect results in the narrowing of the HOMO/LUMO band gap whereas the band bending causes the rigid shift of the HOMO and LUMO levels. To distinguish the metal screening, the HOMO and LUMO should be observed simultaneously by combination of UPS and inverse photoelectron spectroscopy (IPES) [17,18], or scanning tunneling spectroscopy (STS) [19,20]. For example, Kahn and co-workers [18] observed both the highest occupied molecular orbital (HOMO) and lowest unoccupied molecular orbital (LUMO) levels of pentacene films on a polycrystalline gold surface using UPS and IPES as a function of film thickness. They demonstrated that the energy gap at the interface is reduced by approximately 0.7 eV compared with that of bulk pentacene. However, due to the low resolution of and sample damage by IPES, it was difficult to determine the LUMO energy levels precisely. STS, on the other hand, cannot be applied to a thick organic film thus it is not a suitable technique to examine the thickness-dependent HOMO/LUMO energy levels.

We developed low-energy inverse photoelectron spectroscopy (LEIPS) in 2012 [21,22] to solve the problems of low resolution and sample damage in conventional IPES, allowing us to perform very reliable and precise LUMO measurements. In this work, we apply UPS and LEIPS to perylene-3,4,9,10-tetracarboxylic dianhydride (PTCDA) grown on a metal

*Corresponding author: hyoshida@chiba-u.jp

single-crystal surface of Ag(111) and Au(111). In order to quantitatively examine the screening effect of the metal surface from the submonolayer film to the bulk of the organic layer, the film should be grown layer by layer on an atomically flat metal surface. Further, it is known that orientation and crystal structure of organic molecules on metal surface changes as film thickness increases [23], which may also influence the energy levels [24–28]. Thus the orientation of the molecules should not change with the film thickness. In this regard, PTCDA grown on Ag(111) and Au(111) satisfy these conditions. It is known that PTCDA grows in a quasi–layer-by-layer manner and the orientation does not change with increasing film thickness due to intermolecular hydrogen bonds [29]. The observed energy levels are affected not only by the screening effect of the metal surface but also by the interface dipole, band bending, and charge transfer at the surface. In order to extract only information on the screening effect of the metal surface, we employed a procedure we established previously [30,31]. The basic idea is that the response to the positive and negative charges is symmetric in the screening effect or the bandwidth, and antisymmetric in the electrostatic effect, such as interface dipole, charge transfer, molecular orientation, and band bending. From the precisely determined HOMO and LUMO levels, we quantitatively derived the screening energy of the metal surface. Finally, we evaluated the screening energy by comparing it with the value calculated on the basis of the image-charge potential.

II. EXPERIMENTAL METHODS

Sublimed grade PTCDA molecules purchased from Tokyo Chemical Industry Co., Ltd. were used after further purification by vacuum sublimation. The surfaces of Ag(111) and Au(111) were cleaned by cycles of argon ion sputtering and annealing (at approximately 600 K). Cleanliness was confirmed by observing the Shockley state by UPS. Then, the vacuum deposition of PTCDA and UPS, metastable atom electron spectroscopy (MAES), and LEIPS measurements were repeated while increasing the film thickness. The deposition rate was $0.1\,\mathrm{nm\,min^{-1}}$, and the film thickness was increased up to 10 nm. The film thickness was monitored by a quartz crystal microbalance. The thickness of the monolayer was determined to be 0.3 nm from the thickness dependence of the work function and the line shape of MAES spectra. The sample film was not exposed to air during the film preparation and measurements (*in situ* measurements).

UPS spectra were measured with He I light (photon energy $h\nu = 21.22\,\mathrm{eV}$). The vacuum level was determined from the cutoff energy of the secondary electrons. For MAES measurements, metastable He atom (energy of 19.82 eV) was used as the excitation source [32]. The photoelectron energy was analyzed using a PHOIBOS-100 analyzer (SPECS). The energy resolution was about 0.07 eV estimated from the Fermi edge and secondary electron cut off of the polycrystalline Ag film spectrum. The detection angle of the electron beam was set to 0° from the normal to the sample surface for UPS and 60° for MAES. The acceptance angle of the energy analyzer was set to $\pm 9^\circ$. It was reported that the UPS signal intensity at the normal angle is small from the π orbitals of PTCDA with the lying orientation [33]. However, we observed essentially no difference between 0 and 30 ° probably because of the large acceptance angle (see Fig. S1 of the Supplemental Material [34]).

Details of the LEIPS apparatus are described elsewhere [35]. The sample was irradiated with electrons having less than 5 eV kinetic energy perpendicularly to the sample and the emitted light was analyzed using a bandpass filter with a photon energy of 4.785 eV and a photomultiplier tube. The energy resolution was 0.37 eV as estimated by the convolution of electron energy spread (0.24 eV) and the bandwidth of the bandpass filter (0.28 eV). Each measurement took approximately 1 h, and no discernible change of the spectrum was observed during the measurement, indicating no sample damage. The vacuum level was determined from the inflection point of the sample current. The sample preparation and the measurements were performed in vacuum with base pressure lower than 5×10^{-7} Pa.

III. RESULTS

The UPS and LEIPS spectra are shown in Fig. 1. The UPS spectra of PTCDA/Ag(111) [Fig. 1(a)] are in good agreement with the previous reports [33,36,37]. The peak appearing around 0 eV in the UPS spectrum of pristine Ag(111) is attributed to the Shockley state. A peak appears around 0.4 eV in the UPS spectra when 0.2- and 0.3-nm-thick PTCDA is deposited [orange bars in Fig. 1(a)]. This peak was assigned to a LUMO-derived peak occupied by the electron that was transferred from the metal to the molecule. Another peak found around 1.8 eV [green bars in Fig. 1(a)] is assignable to the HOMO of the first layer of PTCDA hybridized with the Ag 4*d* orbital. Above the film thickness of 0.4 nm, the peak around 2.3 eV [indicated by red bars in Fig. 1(a)] is assigned to the HOMO of the second layer of PTCDA [36]. In the LEIPS spectra, the peak at −0.2 eV of pristine Ag(111) is attributed to the Shockley state. Above the film thickness of 0.3 nm, the LUMO peaks are clearly distinguishable [blue bars in Fig. 1(a)].

In the UPS spectra of PTCDA/Au(111) in Fig. 1(b), the peak observed around 2.2 eV at $\geqslant$4.5 nm film thickness is attributed to HOMO and shown by red bars. In the LEIPS spectra, the peaks around −1.4 eV are clearly distinguished at $\geqslant$0.3 nm thickness and attributed to the LUMO-derived state. In both PTCDA/Au(111) and PTCDA/Ag(111), the HOMO peak shifts toward the higher binding energy whereas the LUMO peak shifts toward the lower binding energy with increasing film thickness.

Generally, the HOMO/LUMO energies are determined from the onset of the spectra in UPS or LEIPS measurements. From the spectral onset of the 10-nm-thick PTCDA film, we determined the ionization energies of 6.52 eV on Ag(111) and 6.51 eV on Au(111) and the electron affinities of 4.27 eV on Ag(111) and 4.15 eV on Au(111) corresponding to the HOMO and LUMO energies in the bulk, respectively, with reference to the vacuum level. These values are in good agreement with previous reports (ionization energy [38] and electron affinity [22]). However, the depth of the observed spatial region cannot be specified. In this experiment, we need to examine the energy as a function of the distance between the organic layer and the metal surface. To understand the

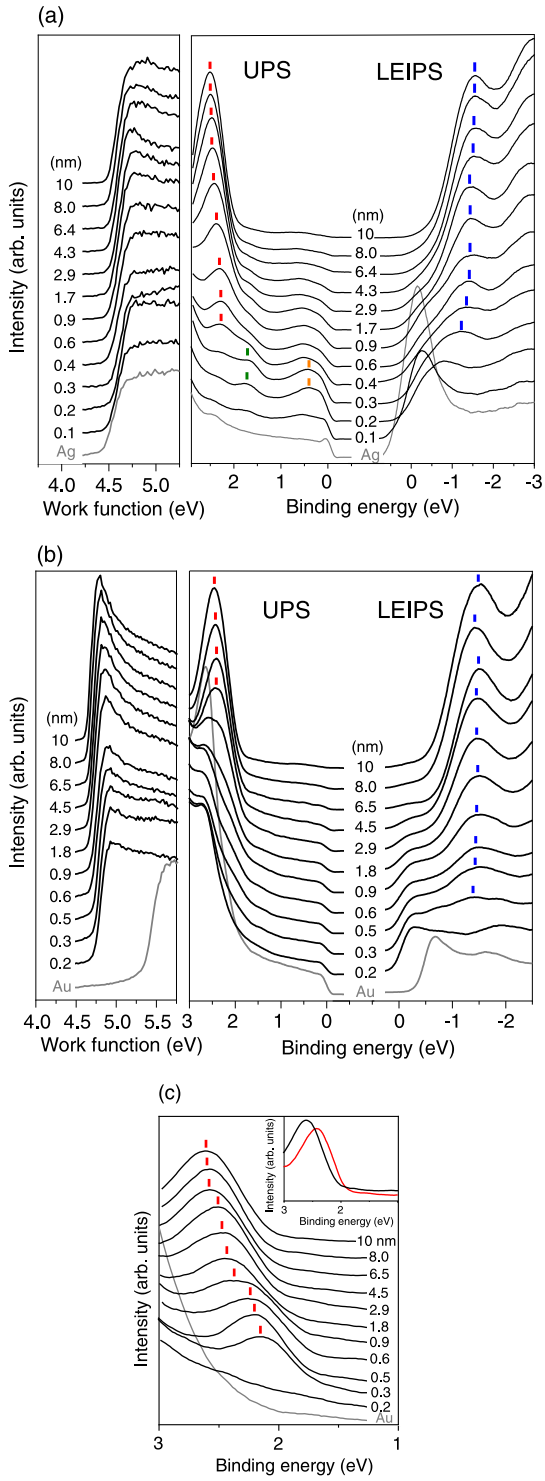

FIG. 1. UPS and LEIPS spectra of PTCDA as a function of film thickness on (a) Ag(111) and (b) Au(111). The right panels show the HOMO and LUMO regions of the UPS and LEIPS spectra, respectively, whereas the left panels show the secondary electron cutoff of UPS, which corresponds to the work function. The thickness of PTCDA is indicated in the figure. The HOMO peaks are indicated by red bars and the LUMO peaks, by blue bars. In the UPS spectra, the occupied LUMO-derived peaks are indicated by orange bars and the peak of PTCDA hybridized with Ag, by green bars. (c) MAES spectra of PTCDA/Au(111) as a function of film thickness. The red bars indicate the HOMO-derived peaks. The inset shows the UPS (red line) and MAES (black line) spectra of 10-nm-thick PTCDA on Au(111).

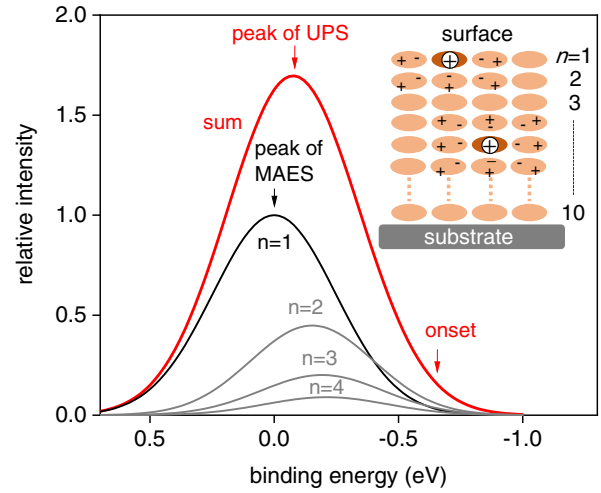

FIG. 2. Simulated UPS spectral line shape of a 10-monolayer film. The peak energy and intensity depend on the layer number n. We assumed that the energy is shifted by the electronic polarization energy [17] and the intensity is attenuated exponentially with the attenuation length of 0.4 nm [41]. The UPS spectrum is simulated as the sum of the signals from each layer which is approximated by a Gaussian function with FWHM of 0.7 eV. The MAES spectrum corresponds to the line shape of the surface layer ($n = 1$).

relationship between the depth and the energy position, we simulated a spectral line shape of PTCDA multilayer (Fig. 2). In the final state of the UPS (LEIPS) process, a hole (electron) is generated in an organic molecule. The photogenerated hole (electron) at the surface layer ($n = 1$) is only partially stabilized whereas that from the bulk layer ($n > 1$) is fully stabilized by the electronic polarization of the surrounding molecules (schematically illustrated by induced dipoles in Fig. 2), leading to the energy level difference between the surface and bulk region of about 0.3 eV [39,40]. In this simulation, we employed calculated polarization energies as a function of layer number n (taken from Fig. 4 of Ref. [17]). On the other hand, the UPS (LEIPS) signal intensity from the bulk layer ($n > 1$) I is attenuated by the upper layers (thickness z) from the initial value I_0 as often approximated by an exponential decay, $I = I_0 \exp(-z/\lambda)$ where the electron attenuation length λ measured for PTCDA/Ag(111) is about 0.4 nm [41]. We used the thickness of the one monolayer of 0.321 nm based on the β-phase single crystal structure [42] for the lying orientation of PTCDA. The spectral line shape of UPS from each layer was approximated by a Gaussian function with the full width at half maximum (FWHM) of 0.7 eV to best reproduce the experimental spectrum.

The UPS spectrum of the whole film was simulated as a sum of the signal from each layer n as shown in Fig. 2. The peak (maximum) of UPS predominantly consists of the signal from the surface layer ($n = 1$). The peak energy of UPS (sum) is slightly shifted (about 0.1 eV) from that of the surface layer toward the low binding energy. Conversely, the onset region of the UPS spectrum is contributed from several layers in the bulk ($n > 1$) with little contribution from the surface. Note that the electron attenuation length for low-energy electrons below

50 eV is under debate [43]. However, this tendency is not altered by a different choice of the attenuation length in the range 0.3–1 nm (Fig. S2 [34]). Therefore, the peak energy of UPS reflects the energy level of the outermost surface layer ($n = 1$) while the onset energy is determined by several layers of the bulk region. To gain higher depth resolution from the UPS and LEIPS data, we analyze the thickness dependence of the peak energy rather than the onset energy.

At a film thickness of less than 3 nm, the HOMO peak could not be distinguished due to the overlap of the Au 5*d* states and the HOMO of PTCDA [37]. In order to determine the HOMO energy of PTCDA on Au(111), we applied MAES. The principle of MAES is similar to that of UPS but ultraviolet photon as the excitation source is replaced by a metastable helium atom [32]. As the helium atom cannot penetrate the sample film, MAES can only observe the outermost molecules of the sample without being affected by the Au(111) substrate. Figure 1(c) shows the MAES spectra of PTCDA/Au(111), where the HOMO-derived peaks are clearly detected even at 0.3 nm thickness (corresponding to monolayer). As we have predicted from the above simulation (Fig. 2), the observed peak energies in the MAES and UPS spectra are slightly different by 0.18 eV in the range 4.5–10 nm of the thickness where the peaks are observed in the both spectra [see the inset of Fig. 1(c)]. Such difference is predicted above bilayer ($n \geqslant 2$). In order to align both results, the energy obtained by MAES spectra was shifted by 0.18 eV toward the lower binding energy except for the one monolayer (0.3 nm).

The HOMO and LUMO energies determined in this way are summarized in Figs. 3(a) and 3(b) as a function of film thickness. The uncertainty of the energy was estimated to be 50 meV from the reproducibility. We observed band gap narrowing at the low film thickness. The results is consistent with the previous UPS/IPES [17,18] and STS [19] results.

IV. DISCUSSION

First, we compared the experimentally obtained HOMO and LUMO energies with the image charge model [Fig. 3(c)]. In this model, the charge q on the molecule is approximated by a point charge. Then, the charge induced on the metal surface can be represented by the image charge $-q$ with the opposite sign located at the distance r symmetrical to the metal surface. If the polarization effect of the organic layer is approximated by that of the dielectric continuum with the relative permittivity ε_r, the potential energy U between the two charges can be expressed as follows:

$$U = -\frac{q^2}{16\pi\varepsilon_0\varepsilon_r r}, \tag{1}$$

where ε_0 is the permittivity of vacuum. We used $\varepsilon_r = 3.32$ for PTCDA calculated on the basis of the molecular polarizability [14]. The distance r between the molecule and the metal surface was calculated as the sum of the distance between the metal surface and the molecule in the first monolayer (0.286 nm for PTCDA/Ag(111) and 0.327 nm for PTCDA/Au(111) measured from x-ray standing waves [44]) and the intermolecular distance of 0.321 nm in the PTCDA crystal of the β phase [42].

In Figs. 3(a) and 3(b), the experimental HOMO and LUMO energies are compared with the values calculated by the image

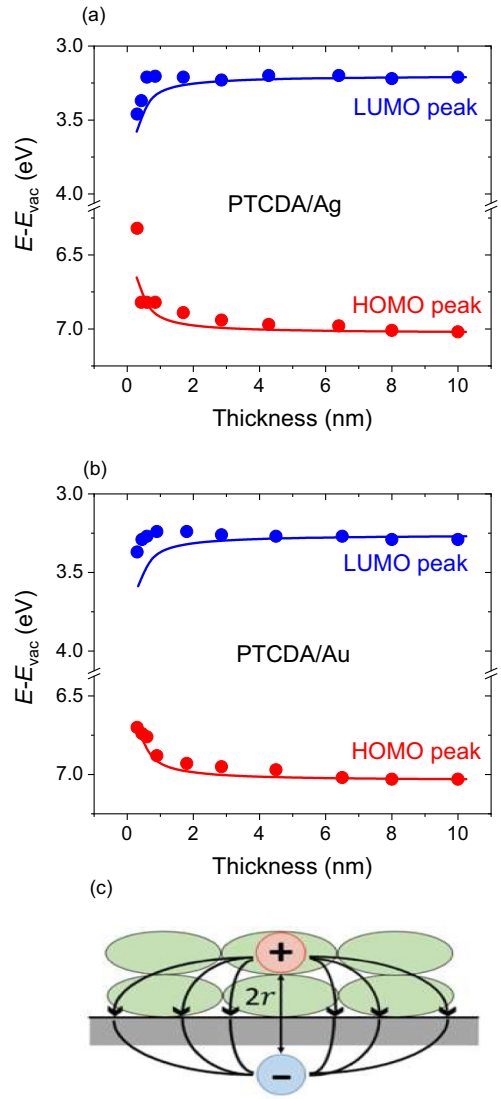

FIG. 3. Experimentally determined energies of the HOMO and LUMO levels (circles) and energies calculated from the image charge model [Eq. (1)] (solid line) as a function of PTCDA film thickness on (a) Ag(111) and (b) Au(111). (c) Schematic diagram of the image charge model.

charge model. The origin of the calculated values (ideally r at infinity) was taken to match the experimental values at $r = 10$ nm. At first glance, the experimental values are in good agreement with the calculated values, indicating that the screening effect of the metal surface can be reproduced by the image charge model. The closer the sample surface is to the metal surface, the narrower the energy gap becomes. On the Ag surface, the energy of the HOMO peak is shifted by 0.2 eV at the second layer [thickness of 0.4–0.6 nm in Figs. 1(a) and 3(a)], and the energy of the LUMO peak, by 0.25 eV at the first layer (0.3 nm) with reference to the corresponding energy at the thickness of 10 nm, resulting in the narrowing of the energy gap by more than 0.45 eV. The HOMO peak of the PTCDA monolayer ($\leqslant$0.3 nm) on Ag is excluded due to the hybridization of the PTCDA with Ag orbitals. On the Au surface, the energy gap is reduced by 0.41 eV at the first layer

[0.3 nm in Figs. 1(b), 1(c), and 3(b)] as a result of the energy shifts of approximately 0.3 and 0.1 eV for the HOMO and LUMO levels, respectively. On close inspection, however, the experimental HOMO and LUMO energies systematically deviate toward the low binding energy side from the calculated values with the decrease of film thickness. This indicates that we have to take effects other than the screening effect into consideration.

In our previous work, we studied the electrostatic interaction energy between the localized charge carrier on a molecule (a temporal molecular ion) and the surrounding molecules by dividing it into electronic polarization energy D and electrostatic energy S [30,31]. The electronic polarization energy D, also referred to as induction or dynamic energy, always stabilizes the system regardless of the positive or negative ion. Conversely, the electrostatic energy S is the Coulomb interaction between the ion and the permanent charge distributed over the surrounding molecules, meaning that the sign of the electrostatic energy depends on that of the ion [45–47]. When the electronic polarization energy and the electrostatic energy are represented by $D_\pm$ and $S_\pm$ (the plus and minus signs correspond to the response to the positive and negative ions, respectively), we can assume that $D_+ = D_-$ and $S_+ = -S_-$. Based on the different dependence on the polarity of the ion, we have established that the electronic polarization energy and the electrostatic energy can be determined from the measured HOMO and LUMO energies. Extending this idea, we analyze the energy levels at the organic/metal interface in terms of the screening effect of the metal surface.

Assuming that the HOMO and LUMO energies of an isolated molecule (the ionization energy I_g and the electron affinity A_g in the gas phase, respectively) are perturbed by the electronic polarization energy (D_+ and D_-) and the electrostatic energy (S_+ and S_-), the HOMO and LUMO energies of the solid (the ionization energy I_s and the electron affinity A_s in the solid phase, respectively) are expressed as [27]

$$\begin{aligned} I_\mathrm{s} &= I_\mathrm{g} - (D_+ + S_+) - \Delta_+, \\ A_\mathrm{s} &= A_\mathrm{g} + (D_- + S_-) + \Delta_-, \end{aligned} \tag{2}$$

where Δ_+ and Δ_- are the corrections due to the quantum mechanical interactions for the HOMO and LUMO levels, respectively. If we assume the relationship mentioned above, $D \equiv D_+ = D_-$ and $S \equiv S_+ = -S$, the electronic polarization energy D and the electrostatic energy S can be calculated as follows:

$$\begin{aligned} D &= \frac{-(I_\mathrm{s} - A_\mathrm{s}) + (I_\mathrm{g} - A_\mathrm{g}) - (\Delta_+ + \Delta_-)}{2}, \\ S &= \frac{-(I_s + A_\mathrm{s}) + (I_\mathrm{g} + A_\mathrm{g}) - (\Delta_+ - \Delta_-)}{2}. \end{aligned} \tag{3}$$

We apply this model to the metal/organic interface energy levels. The screening effect of the metal surface always stabilizes the charges regardless of the polarity of the ion, meaning that it is calculated as D from Eq. (3). At the metal/organic interface, the interface dipole layer [1] and the band bending [3] can be dominant effects. These affect the HOMO and LUMO levels similarly and are thus calculated as S in Eq. (3). We can extract the screening effect of the metal surface from other major effects that occur at the interface using Eq. (3). We use $I_g = 8.2$ eV measured by gas UPS [48] and $A_g = 3.07$ eV [49] determined by density functional theory (DFT) calculation with the B3LYP functional. It was reported that the bandwidths between HOMO and LUMO are similar from the band structure calculation [50] and the bandwidth of HOMO is approximately 0.2 eV as observed from energy-dependent photoelectron spectroscopy [51]. Thus, the contribution from the quantum effect is neglected in S because Δ_+ and Δ_- are canceled out. For the electronic polarization energy D, on the other hand, the correction due to the quantum effect Δ_+ and Δ_- is small but necessary. Usually, we assume that $\Delta_\pm$ is half of the bandwidth in the bulk. In this work, we discuss the energy levels at the surface. The nature of the band structure of the PTCDA film is one dimensional along the molecular stacking direction, which is normal to the surface [50,51]. The bandwidth of the truncated one-dimensional band at the surface becomes half of that in the bulk PTCDA because the band structure of an organic solid is well approximated by the tight-binding model [52,53]. We therefore assume that the quantum mechanical contribution to D in Eq. (3) is a quarter of the bandwidth in the bulk, $\Delta_+ = \Delta_- = 0.05$ eV.

The obtained D and S are shown in Fig. 4. The D values for PTCDA/Ag(111) and PTCDA/Au(111) are also compared with the image charge model based on Eq. (1). D is contributed from the screening of the metal surface and the electronic polarization of the organic layer. The former depends on the thickness according to Eq. (1), which shows excellent agreement. The latter contribution from the organic layer is almost constant and is around 0.5 eV which is smaller than the previous values of 1 eV [30,31], which can be understood from the discussion above (Fig. 2); we evaluated D for the bulk value derived from the onset of HOMO and LUMO peaks in the previous studies, whereas the surface values derive from the maximum of HOMO and LUMO peaks are used in the present work. The difference of approximately 0.5 eV is twice the difference of 0.25 eV between the surface and bulk in each HOMO or LUMO level. The value is good agreement with the surface/bulk energy shift of about 0.3 eV for the core levels measured by angle-resolved x-ray photoelectron spectroscopy [40].

The contribution from the electronic polarization of organic layers can be further discussed in comparison with the previous calculation by Soos and co-workers for the screening effect of the metal surface with PTCDA [17]; they treated the screening effect of metal and molecules by the image-charge potential and the polarizability of each molecule, respectively, and calculated the electronic polarization energy $D_+ + D_- = 2D$ of PTCDA at one, two, three, five, and ten layers and semi-infinite thicknesses on the metal surface. Therefore, this calculation takes the effect of the molecular polarization into consideration more accurately than the continuous dielectric model used in Eq. (1). The comparison is shown in Figs. 4(a) and 4(b). As the calculations were carried out for different adsorption distances r_1, the calculated result that is most consistent with r_1 obtained from the x-ray standing waves [44] was used. The origin of the calculated values was shifted so that the values matched with the experimental values. The comparison in Figs. 4(a) and 4(b) shows that both models are in good agreement with the experimental results. Comparing the two calculations, we find that the precise calculation shows slightly better agreement with the

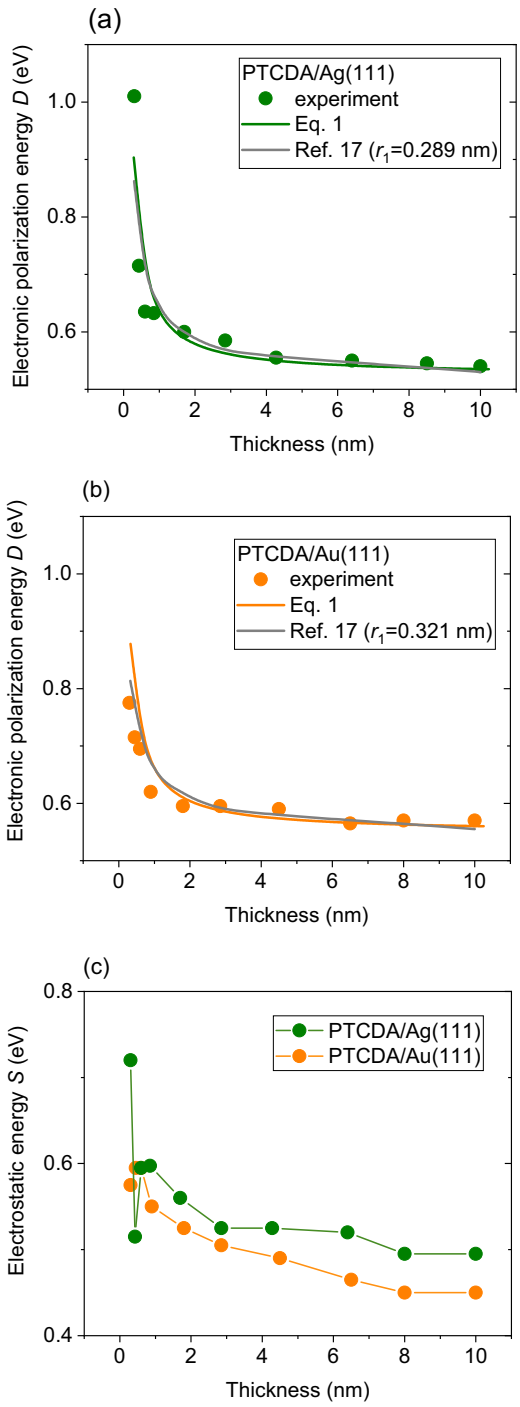

FIG. 4. Electronic polarization energy D [Eq. (3)] for PTCDA on (a) Ag(111) and (b) Au(111), respectively. Values obtained from the experiments are shown in circles, whereas the calculation values using Eq. (1) and those taken from Ref. [17] are shown by solid lines, where r_1 is the adsorption distance of first-layer PTCDA [44]. (c) Electrostatic energy S [Eq. (3)].

experimental results. However, the effect of the electronic polarization energy of the molecules is much smaller than the metal screening effect. The simple image charge model with continuous dielectric media [Eq. (1)] is considered to be a good approximation of the screening effect of the metal surface.

The screening effect of the metal surface D obtained from the experimental values is in good agreement with the calculated values based on the image charge model. This suggests that the discrepancy between the experimental values and the values calculated on the basis of the image charge model in Figs. 3(a) and 3(b) is caused by the electrostatic energy S. As shown in Fig. 4(c), the value of S in the thin film near the monolayer (about 0.3 nm in thickness) is larger than the value in the thick film. The thickness dependence of S may be caused by the molecular distortion at the surface. It has been reported using the x-ray standing wave that the O atoms are distorted to the vacuum side in the first-layer PTCDA on Ag(111) [44]. The position of the O atoms in PTCDA on Au(111) could not be measured due to an overlap of Au Auger lines with the O 1s core level in the x-ray standing wave [54]. However, if we consider that even a small amount of O atom distortion has occurred, we can infer that S in the thin film is larger due to the dipole effect caused by the distortion. The difference in the value of the electrostatic energy between the thin and thick films may be due to a slight difference in molecular orientation and crystal structure. When deposited at room temperature, thick films of PTCDA on Ag are known to be composed of a mixture of α and β phases [55].

V. CONCLUSION

We have investigated the screening effect of the metal surface at the organic/metal interface by examining the HOMO and LUMO levels of PTCDA on Ag(111) and Au(111). By applying our previous procedure for separating the electronic polarization energy and the electrostatic energy [30,31], we were able to extract the contribution of the metal screening effect as the electronic polarization energy (also referred to as the induction or dynamic energy) D. The change in energy level alignment due to the screening effect of the metal surface was found to be as much as 0.25 eV at the first layer in the vicinity of the metal surface. This means that the screening effect has a significant impact on the charge injection/extraction barrier at the metal/organic interface.

We also demonstrated that the energy of metal screening effect can be precisely reproduced by the image charge model. Predicting the metal screening energy by this simple model is useful in practice. For example, the charge injection/extraction barrier at the metal/organic interface is often predicted from the work function of metal and the ionization energy/electron affinity of organic material. As a correction to this simple estimation, the metal screening energy can be calculated. For more precise analysis, the energy level alignment at the interface is examined using UPS. The observed thickness-dependent energy levels contain the contribution from the metal screening effect which cannot be identified from the UPS data alone but can be evaluated from the image potential model. Regarding the first principle calculation, the electronic polarization energy of dielectric materials can be obtained by the GW approximation [30,31]. However, the first principle method is still difficult to accurately calculate the metal screening energy. Our results assure that the screening energy of metal surface can reliably be computed as additional energy by the classical image charge model.

ACKNOWLEDGMENT

This work was supported by the Futaba Foundation's Futaba Research Grant Program.

T.A. and S.A.A.-R. performed the measurements. T.A. analyzed the data. H.Y. conceived the original idea and supervised the project. T.A., S.A.A.-R., and H.Y. wrote the manuscript.

[1] H. Ishii, K. Sugi yama, E. Ito, and K. Seki, Energy level alignment and interfacial electronic structures at organic/metal and organic/organic interfaces, Adv. Mater. **11**, 605 (1999).

[2] S. Braun, W. R. Salaneck, and M. Fahlman, Energy-level alignment at organic/metal and organic/organic interfaces, Adv. Mater. **21**, 1450 (2009).

[3] M. Oehzelt, N. Koch, and G. Heimel, Organic semiconductor density of states controls the energy level alignment at electrode interfaces, Nat. Commun. **5**, 4174 (2014).

[4] A. Franco-Cañellas, S. Duhm, A. Gerlach, and F. Schreiber, Binding and electronic level alignment of π-conjugated systems on metals, Rep. Prog. Phys. **83**, 066501 (2020).

[5] M. Knupfer and H. Peisert, Electronic properties of interfaces between model organic semiconductors and metals, Phys. Status Solidi **201**, 1055 (2004).

[6] D. Cahen, A. Kahn, and E. Umbach, Energetics of molecular interfaces, Mater. Today **8**, 32 (2005).

[7] N. Koch, Energy levels at interfaces between metals and conjugated organic molecules, J. Phys.: Condens. Matter **20**, 184008 (2008).

[8] F. Flores, J. Ortega, and H. Vázquez, Modelling energy level alignment at organic interfaces and density functional theory, Phys. Chem. Chem. Phys. **11**, 8658 (2009).

[9] Y. Gao, Surface analytical studies of interfaces in organic semiconductor devices, Mater. Sci. Eng. R Rep. **68**, 39 (2010).

[10] G. D'Avino, L. Muccioli, F. Castet, C. Poelking, D. Andrienko, Z. G. Soos, J. Cornil, and D. Beljonne, Electrostatic phenomena in organic semiconductors: fundamentals and implications for photovoltaics, J. Phys.: Condens. Matter **28**, 433002 (2016).

[11] A. Tan and P. Zhang, Tailoring the growth and electronic structures of organic molecular thin films, J. Phys.: Condens. Matter **31**, 503001 (2019).

[12] C. J. Brabec, N. S. Sariciftci, and J. C. Hummelen, Plastic solar cells, Adv. Funct. Mater. **11**, 15 (2001).

[13] M. Schaal, T. Aihara, M. Gruenewald, F. Otto, J. Domke, R. Forker, H. Yoshida, and T. Fritz, Hybridization vs decoupling: influence of an h-BN interlayer on the physical properties of a lander-type molecule on Ni(111), Beilstein J. Nanotechnol. **11**, 1168 (2020).

[14] J. Tsutsumi, H. Yoshida, R. Murdey, S. Kato, and N. Sato, An accurate calculation of electronic contribution to static permittivity tensor for organic molecular crystals on the basis of the charge response kernel theory, J. Phys. Chem. A **113**, 9207 (2009).

[15] I. G. Hill, A. J. Mäkinen, and Z. H. Kafafi, Initial stages of metal/organic semiconductor interface formation, J. Appl. Phys. **88**, 889 (2000).

[16] M. G. Helander, M. T. Greiner, Z. B. Wang, and Z. H. Lu, Effect of electrostatic screening on apparent shifts in photoemission spectra near metal/organic interfaces, Phys. Rev. B **81**, 153308 (2010).

[17] E. V. Tsiper, Z. G. Soos, W. Gao, and A. Kahn, Electronic polarization at surfaces and thin films of organic molecular crystals: PTCDA, Chem. Phys. Lett. **360**, 47 (2002).

[18] F. Amy, C. Chan, and A. Kahn, Polarization at the gold/pentacene interface, Org. Electron. **6**, 85 (2005).

[19] J. Repp, G. Meyer, S. M. Stojković, A. Gourdon, and C. Joachim, Molecules on Insulating Films: Scanning-Tunneling Microscopy Imaging of Individual Molecular Orbitals, Phys. Rev. Lett. **94**, 026803 (2005).

[20] I. Fernández Torrente, K. J. Franke, and J. Ignacio Pascual, Spectroscopy of C 60 single molecules: The role of screening on energy level alignment, J. Phys.: Condens. Matter **20**, 184001 (2008).

[21] H. Yoshida, Near-ultraviolet inverse photoemission spectroscopy using ultra-low energy electrons, Chem. Phys. Lett. **539–540**, 180 (2012).

[22] H. Yoshida, Principle and application of low energy inverse photoemission spectroscopy: A new method for measuring unoccupied states of organic semiconductors, J. Electron. Spectrosc. Relat. Phenom. **204**, 116 (2015).

[23] G. Witte and C. Wöll, Growth of aromatic molecules on solid substrates for applications in organic electronics, J. Mater. Res. **19**, 1889 (2004).

[24] H. Yamane, Y. Yabuuchi, H. Fukagawa, S. Kera, K. K. Okudaira, and N. Ueno, Does the molecular orientation induce an electric dipole in cu-phthalocyanine thin films?, J. Appl. Phys. **99**, 093705 (2006).

[25] S. Duhm, G. Heimel, I. Salzmann, H. Glowatzki, R. L. Johnson, A. Vollmer, J. P. Rabe, and N. Koch, Orientation-dependent ionization energies and interface dipoles in ordered molecular assemblies, Nat. Mater. **7**, 326 (2008).

[26] W. Chen, H. Huang, S. Chen, Y. L. Huang, X. Y. Gao, and A. T. S. Wee, Molecular orientation-dependent ionization potential of organic thin films, Chem. Mater. **20**, 7017 (2008).

[27] H. Yoshida, K. Yamada, J. Tsutsumi, and N. Sato, Complete description of ionization energy and electron affinity in organic solids: determining contributions from electronic polarization, energy band dispersion, and molecular orientation, Phys. Rev. B **92**, 075145 (2015).

[28] A. Sugie, W. Han, N. Shioya, T. Hasegawa, and H. Yoshida, Structure-dependent electron affinities of perylene diimide-based acceptors, J. Phys. Chem. C **124**, 9765 (2020).

[29] L. Chkoda, M. Schneider, V. Shklover, L. Kilian, M. Sokolowski, C. Heske, and E. Umbach, Temperature-dependent morphology and structure of ordered 3,4,9,10-perylene-tetracarboxylicacid-dianhydride (PTCDA) thin films on Ag(1 1 1), Chem. Phys. Lett. **371**, 548 (2003).

[30] K. Yamada, S. Yanagisawa, T. Koganezawa, K. Mase, N. Sato, and H. Yoshida, Impact of the molecular quadrupole moment on ionization energy and electron affinity of organic thin films:

experimental determination of electrostatic potential and electronic polarization energies, Phys. Rev. B **97**, 245206 (2018).

[31] Y. Uemura, S. A. Abd-Rahman, S. Yanagisawa, and H. Yoshida, Quantitative analysis of the electrostatic and electronic polarization energies in molecularly mixed films of organic semiconductors, Phys. Rev. B **102**, 125302 (2020).

[32] Y. Harada, S. Masuda, and H. Ozaki, Electron spectroscopy using metastable atoms as probes for solid surfaces, Chem. Rev. **97**, 1897 (1997).

[33] M. Willenbockel, D. Lüftner, B. Stadtmüller, G. Koller, C. Kumpf, S. Soubatch, P. Puschnig, M. G. Ramsey, and F. S. Tautz, The interplay between interface structure, energy level alignment and chemical bonding strength at organic–metal interfaces, Phys. Chem. Chem. Phys. **17**, 1530 (2015).

[34] See Supplemental Material at http://link.aps.org/supplemental/10.1103/PhysRevB.104.085305 for the effect of the detection angle in UPS measurements and the simulation of UPS and MAES spectra with different attenuation lengths.

[35] H. Yoshida, Note: low energy inverse photoemission spectroscopy apparatus, Rev. Sci. Instrum. **85**, 016101 (2014).

[36] Y. Zou, L. Kilian, A. Schöll, T. Schmidt, R. Fink, and E. Umbach, Chemical bonding of PTCDA on Ag surfaces and the formation of interface states, Surf. Sci. **600**, 1240 (2006).

[37] S. Duhm, A. Gerlach, I. Salzmann, B. Bröker, R. L. Johnson, F. Schreiber, and N. Koch, PTCDA on Au(111), Ag(111) and Cu(111): Correlation of interface charge transfer to bonding distance, Org. Electron. **9**, 111 (2008).

[38] Y. Hirose, W. Chen, E. I. Haskal, S. R. Forrest, and A. Kahn, Structural and electronic properties of an organic/inorganic semiconductor interface: PTCDA/GaAs(100), J. Vac. Sci. Technol. B **12**, 2616 (1994).

[39] Y. Harada, H. Ozaki, and K. Ohno, Selective Observation of Outermost Surface Layer During Epitaxial Growth by Penning-Ionization Electron Spectroscopy: Pentacene on Graphite, Phys. Rev. Lett. **52**, 2269 (1984).

[40] H. Yoshida and N. Sato, A precise analysis of the core-level energy difference between the surface and bulk region of organic semiconductor thin films, J. Phys. Chem. C **116**, 10033 (2012).

[41] T. Graber, F. Forster, A. Schöll, and F. Reinert, Experimental determination of the attenuation length of electrons in organic molecular solids: The example of PTCDA, Surf. Sci. **605**, 878 (2011).

[42] M. Möbus, N. Karl, and T. Kobayashi, Structure of perylene-tetracarboxylic-dianhydride thin films on alkali halide crystal substrates, J. Cryst. Growth **116**, 495 (1992).

[43] Y. Ozawa, Y. Nakayama, S. Machida, H. Kinjo, and H. Ishii, Maximum probing depth of low-energy photoelectrons in an amorphous organic semiconductor film, J. Electron. Spectrosc. Relat. Phenom. **197**, 17 (2014).

[44] A. Gerlach, S. Sellner, F. Schreiber, N. Koch, and J. Zegenhagen, Substrate-dependent bonding distances of PTCDA: A comparative x-ray standing-wave study on Cu(111) and Ag(111), Phys. Rev. B **75**, 045401 (2007).

[45] P. J. Bounds and R. W. Munn, Polarization energy of a localized charge in a molecular crystal. II. charge-quadrupole energy, Chem. Phys. **59**, 41 (1981).

[46] N. Sato, H. Inokuchi, and E. A. Silinsh, Reevaluation of electronic polarization energies in organic molecular crystals, Chem. Phys. **115**, 269 (1987).

[47] B. J. Topham and Z. G. Soos, Ionization in organic thin films: electrostatic potential, electronic polarization, and dopants in pentacene films, Phys. Rev. B **84**, 165405 (2011).

[48] N. Dori, M. Menon, L. Kilian, M. Sokolowski, L. Kronik, and E. Umbach, Valence electronic structure of gas-phase 3,4,9,10-perylene tetracarboxylic acid dianhydride: Experiment and theory, Phys. Rev. B **73**, 195208 (2006).

[49] P. K. Nayak and N. Periasamy, Calculation of electron affinity, ionization potential, transport gap, optical band gap and exciton binding energy of organic solids using 'Solvation' model and DFT, Org. Electron. **10**, 1396 (2009).

[50] S. Sharifzadeh, A. Biller, L. Kronik, and J. B. Neaton, Quasiparticle and optical spectroscopy of the organic semiconductors pentacene and PTCDA from first principles, Phys. Rev. B **85**, 125307 (2012).

[51] H. Yamane, S. Kera, K. K. Okudaira, D. Yoshimura, K. Seki, and N. Ueno, Intermolecular energy-band dispersion in PTCDA multilayers, Phys. Rev. B **68**, 033102 (2003).

[52] Y. Kashimoto, K. Yonezawa, M. Meissner, M. Gruenewald, T. Ueba, S. Kera, R. Forker, T. Fritz, and H. Yoshida, The evolution of intermolecular energy bands of occupied and unoccupied molecular states in organic thin films, J. Phys. Chem. C **122**, 12090 (2018).

[53] H. Yoshida and N. Sato, Crystallographic and electronic structures of three different polymorphs of pentacene, Phys. Rev. B **77**, 235205 (2008).

[54] S. K. M. Henze, O. Bauer, T.-L. Lee, M. Sokolowski, and F. S. Tautz, Vertical bonding distances of PTCDA on Au(111) and Ag(111): Relation to the bonding type, Surf. Sci. **601**, 1566 (2007).

[55] L. Kilian, E. Umbach, and M. Sokolowski, Molecular beam epitaxy of organic films investigated by high resolution low energy electron diffraction (SPA-LEED): 3,4,9,10-Perylenetetracarboxylicacid-Dianhydride (PTCDA) on Ag(111), Surf. Sci. **573**, 359 (2004).